

Viscous Sintering of Acid Leached Glass Powders

R. Gomes Fernandes¹, R. Al-Mukadam¹, H. Bornhöft¹, S. Reinsch², R. Müller²,
S. Selle³, and J. Deubener^{1*}

¹ Clausthal University of Technology, Institute of Non-Metallic Materials, 38678 Clausthal-Zellerfeld, Germany

² Bundesanstalt für Materialforschung und -prüfung (BAM), 12489 Berlin, Germany

³ Fraunhofer Institute for Microstructure of Materials and Systems IMWS, 06120 Halle, Germany

*Correspondence: joachim.deubener@tu-clausthal.de

Abstract. The process of viscous flow sintering is a phenomenon that is closely linked to the surface properties of the glass particles. In this work, we studied the extreme case of acid-leaching of soda-lime-silicate glass beads of two different particle size distributions and its effects on non-isothermal viscous sintering of powder compacts. Depth profiling of the chemical composition after leaching revealed a near-surface layer depleted in alkali and alkaline earth ions, associated with concurrent hydration as mass loss was detected by thermogravimetry. Heating microscopy showed that acid treatment of glasses shifted the sinter curves to higher temperatures with increasing leaching time. Modelling of the shrinkage with the cluster model predicted a higher viscosity of the altered surface layer, while analysis of the time scales of mass transport of mobile species (Na^+ , Ca^{2+} and H_2O) during isochronous sintering revealed that diffusion of Na^+ can compensate for concentration gradients before sintering begins. Also, exchanged water species can diffuse out of the altered layer, but the depletion of Ca^{2+} in the altered surface layer persists during the sinter interval, resulting in a glass with higher viscosity, which causes sintering to slow down.

Keywords: Glass powder, Viscous sintering, Acid-leaching, Sinter retardation

1. Introduction

Sintering of glass powder is used in many industrial applications, e.g. dental glass-ceramics [1], [2], marble-like tiles for architecture and construction [3], solder glasses [4], fibre-reinforced glasses [5], electronic substrates [6], [7], 3D printed objects [8], [9], three-dimensional translucent scaffolds for photocatalysis/optical sensors [9] and vitreous enamel coatings [10], [11]. During processing, glass powders are often exposed to aqueous solutions to produce slips and slurries, which are basic components of wet coating technologies [1], [10]. Various reactions can occur that lead to chemical and physical alterations of the glass surface [12], [13]. For example, ion exchange reactions between Na^+ in the glass and H^+ in the solution, water molecules diffusing into the glass, or hydrogen containing species reacting with non-bridging oxygen on the surface [14], [15], [16]. The mechanisms and rate-controlling processes at the glass surface can depend on the glass composition, homogeneity, surface preparation, ambient media, atmosphere, temperature and time [12], [13], [17]. For example, an alkali-deficient hydrated (leached) layer with altered viscosity and surface energy can form under the glass surface. Since viscous sintering is driven by the reduction of the surface energy of the compacted powder and limited by the viscous flow at the surface of the powder particles, corrosion

and leaching phenomena are of crucial importance for the sintering progress. In practice, insufficient surface quality of fired products is empirically corrected by parameters at the furnace, while only recently a first knowledge-based study on diffusive mass transfer during sintering of hydrated glass powders was available [18].

Against this background, we focus on the sintering kinetics of acid leached soda-lime-silicate glass beads studied for different particle size distributions and leaching times. The results are discussed based on viscometry, electron microscopy, chemical depth profiling, differential scanning calorimetry, thermogravimetry and mass spectrometry degassing measurements with the aim of providing a prediction of the sintering progress of glass particle compacts with altered surface chemistry.

2. Material and methods

2.1 Glass powders

Small and large soda-lime-silicate glass beads (Potters Industries, Fleurus, Belgium), supplied as Spherglass® 5000 and Spherglass® 2429 respectively, were used for the present study and will hereafter be referred to as 5000 and 2429 for short. To prepare coarse powder samples, 500 g of glass 2429 was sieved three times to $> 45 \mu\text{m}$ and washed three times with isopropanol using a $45 \mu\text{m}$ square metal grid to remove the undersize fraction. The fine glass powder samples were taken from glass 5000 as received. To prepare bulk reference samples, 200 g of glass 2429 was heated in an electric furnace (LHT04/17, Naberthem, Lilienthal, Germany) at 1773 K for 4 hours and quenched in air.

2.2 Chemical analysis and particle size distribution and glass density

For chemical analysis, 3 g of the coarse and fine powder were dissolved in lithium tetraborate flux. Chemical analysis of the melt product was performed using an X-ray fluorescence spectrometer (S4 Pioneer, Bruker AXS, Karlsruhe, Germany) based on calibration curves for SiO_2 , Al_2O_3 , Fe_2O_3 , MnO , MgO , CaO , Na_2O , K_2O , TiO_2 , P_2O_5 . The particle size distribution (PSD) of the powders was measured by laser diffraction (LS230, Coulter, Miami, USA), while a helium pycnometer (Pycnomatic ATC EVO, Porotec, Hofheim, Germany) was used to determine the glass density. The standard deviation based on several measurements was $\pm 0.005 \text{ g cm}^{-3}$.

2.3 Acid-leaching and electron microscopy

Fine and coarse powders were leached in an acidic solution of HNO_3 (1 mol l^{-1}) at 363 K in a sealed polyethylene container containing 1 g of glass spheres and 30 ml of acid for 1 to 24 hours. Scanning electron microscopy (SEM) and energy dispersive X-ray spectroscopy (SEM-EDXS) on mechanically polished cross-sections of the sintered compacts (leached and unleached) were performed using a SEM (Sigma 300 Zeiss, Oberkochen, Germany) equipped with an EDXS detector (Ultim Max 40, Oxford Instruments, Abingdon, UK) for elemental mapping at 8 and 20 keV. Spectra acquisition and further quantitative processing of the EDXS data were performed using Aztec software (version 6.1, Oxford Instruments, Abingdon, UK).

2.4 Chemical depth profiling

Before and after leaching, a depth profile of the chemical composition from the surface to the core of the glass beads was obtained using an electron gas secondary neutral mass spectroscope (SNMS, INA-X SPECS, Berlin, Germany). The samples were prepared by pressing glass beads onto an indium foil, removing the unfixed material with a hoover and covering the edge with a copper mask. The area studied had a diameter of 5 mm and was sputtered with Kr^+ plasma with an energy of 500 eV in high frequency mode (1000 kHz, 60% duty cycle).

Since it was difficult to measure the depth of the sputtered crater on the sample consisting of several spherical glass spheres, the sputtering rate for flat soda-lime-silicate glass of 0.3 nm s^{-1} [19] was used to convert time to depth. It should be noted that the atomic sputtering process is independent of the curvature of the glass surface.

2.5 Thermal analysis and sintering

Differential scanning calorimetry (DSC) was performed with a DSC 404 F3 Pegasus instrument (Netzsch, Selb, Germany) in air atmosphere (100 ml min^{-1}). Powder samples ($\sim 25 \text{ mg}$) were subjected to the heating-cooling-heating programme from room temperature to 1065 K at a heating and cooling rate of 10 K min^{-1} in PtRh20 crucibles with lids. Prior to this, the baseline was corrected using two identical but empty PtRh20 crucibles with lids. Temperature calibration was performed using the melting temperatures of pure In, Bi, Zn, Al, Ag, Au and Sn in corundum-coated Pt crucibles of the same geometry. Thermogravimetry and volatile species analysis by mass spectrometry (STA-MS, 409 PC Luxx, Netzsch, Selb, Germany) was performed on powder samples ($\sim 100 \text{ mg}$) by heating in an Al_2O_3 crucible and air atmosphere (50 ml min^{-1}) using the same time-temperature protocol as for DSC measurements. Temperature calibration was performed by measuring three times the melting temperatures of the pure metals In, Zn, Al and Au in corundum crucibles. The error associated with weight loss was determined based on the standard deviation of the total weight loss of three measurements of unleached fine powder and was $\pm 0.03 \text{ mg}$.

For the shrinkage measurements, powder compacts were prepared by placing ~ 32 and $\sim 30 \text{ mg}$ of fine and coarse powder, respectively, into a cylindrical mould of 3 mm diameter and height. The powder was then carefully and repeatedly compacted with a soft spring plunger, and three drops of ethanol were added as a binder. The sintering of the compact was measured using a heating microscope (Hesse Instruments, Osterode, Germany) with optical data acquisition and image analysis at a heating of 10 K min^{-1} . The temperature calibration was based on the melting points of the pure bulk metals Zn, Al and Ag. The temperature standard deviation of three measurements was $\pm 3 \text{ K}$.

The early stage of sintering up to $t_{0.8}$ (= time to reach a relative density ρ of 0.8) was modelled using the Frenkel approach [20] for the coalescence of two glass spheres, which determines the linear sintering rate $s' = ds/dt$, where s is the linear shrinkage, by equating the energy gain from the decrease in surface area with the dissipated energy of the viscous flow. The Frenkel model is often expressed in the form [21]:

$$s' = \frac{3\gamma}{8\eta r_0} k_f \quad (1)$$

with γ = surface energy, η = viscosity, r_0 = particle radius and k_f = particle shape factor (= 1 for spherical particles). The later stage of sintering (isolated pores, $t > t_{0.8}$) was modelled using the Mackenzie-Shuttleworth approach [22]. For the relative densification rate $\rho' = d\rho/dt$, where ρ is the relative density of the compact, one has [23]:

$$\rho' = \frac{3\gamma}{\eta} \left(\frac{O^{1/3}}{2r_0} \right) (1 - \rho)^{2/3} \rho^{1/3} \quad (2)$$

with O = number of pores per particle. Eq. (1) and (2) were combined for numerical integration of the entire linear shrinkage. Using the conversion for isotropic sintering $\rho_0/\rho = V/V_0 = (1-s)^3$, which results in $s = 1 - (\rho_0/\rho)^{1/3}$ and $s'/\rho' = \rho_0^{1/3}/3\rho^{4/3}$, respectively and relating $O^{1/3} \approx 2k_f$ one may integrate [5]:

$$s(t) = \int_0^{t_{0.8}} s'(\xi) d\xi + \int_{t_{0.8}}^t \rho'(\xi) \left[\frac{\rho_0^{1/3}}{3\rho(\xi)^{4/3}} \right] d\xi \quad (3)$$

For a narrow particle size distribution (PSD), preferred interaction (contacts) of glass particles of the same size have been assumed so far in literature [24]. In this cluster model, sintering is described as a superposition of the contribution of each particle size, weighed by its relative frequency $\Psi(r_{0j})$ of the PSD according to [24]:

$$s \approx \sum_j \Psi_j(r_{0j}) s_j \quad (4)$$

with s_j = shrinkage of powder fraction j .

2.6 Viscometry

Bulk samples of reshaped glass 2429 were cut for the determination of high and medium viscosity. For high viscosities ($10^{10.3}$ – $10^{12.1}$ Pa s), a vertical dilatometer (Bähr VIS 404, Hüllhorst, Germany) with a micropenetration setup was used. For this, a polished glass plate (2.75 mm thick) was placed under a SiO₂ glass rod, which pressed a sapphire ball (1.5 mm diameter) into the glass sample at the target temperature and under a load of 400 g. Medium viscosities ($10^{8.5}$ – 10^{10} Pa s) were determined with a horizontal dilatometer (Bähr VIS 401, Hüllhorst, Germany) in a symmetric three-point bending mode setup. For this purpose, a rod of approximately $43 \times 3 \times 4$ mm³ was bent during heated at 10 K min⁻¹. Low viscosity measurements ($10^{1.3}$ – $10^{2.7}$ Pa s) were performed in a concentric-cylinder rheometer (Haake RV 20, Karlsruhe, Germany) using 40 g of glass beads. The experimental procedures for measuring the viscosity of these three methods, including temperature calibration, are described in detail in [25], [26]. The certified viscosity data of DGG-I glass [27] were reproduced with a standard deviation of ± 0.1 , ± 0.05 and ± 0.02 in log units for micropenetration, beam-bending and concentric cylinder measurements, respectively. Finally, the MYEGA model was used to describe the temperature-dependent viscosity $\eta(T)$ [28]:

$$\log \eta(T) = A + (12 - A) \frac{T_{12}}{T} \exp \left[\left(\frac{m}{12 - A} - 1 \right) \left(\frac{T_{12}}{T} - 1 \right) \right] \quad (5)$$

where the three adjustable parameters are $A = \log \eta_\infty$ (viscosity in the high temperature limit), m (kinetic fragility) and T_{12} (viscometric glass transition temperature = $T(10^{12}$ Pa s)).

2.7 Surface energy

The surface energy of glass 2429 was determined by the pendant drop method using a heating microscope (Hesse Instruments, Osterode, Germany) with optical data acquisition. A block (0.2–0.3 g) of reshaped glass 2429 was placed on a Pt wire loop, flowed through the loop and formed a hanging drop at temperatures between 1102 and 1364 K. The surface energy was then determined from the mass (density times volume) and shape of the pendant drop based on the Young-Laplace equation using the dpiMAX software of the contour analysis system (OCA 15plus, Data Physics, Filderstadt, Germany). The density was corrected for the thermal expansion of the liquefied glass, using typical coefficient of thermal expansion values of 9 and 27 ppm K⁻¹ for temperatures below and above the glass transition, respectively.

3. Results

Chemical composition analysis revealed that glasses 5000 and 2429, which were used to prepare fine and coarse powders, had only minor differences of 0.3 and 0.9 wt% for CaO and MgO, respectively (Tab. 1). The difference in glass density, i.e. 2.472 g cm⁻³ for glass 5000 and 2.475 g cm⁻³ for glass 2429 was within the measurement error.

Fitting Eq. (5) to the viscosity data of the glass 2429 gave the parameters values $A = -1.30 \pm 0.05$, $m = 38.9 \pm 0.2$ and $T_{12} = 834.3 \pm 0.3$ K (Fig. 1). It was assumed that these values also apply to glass 5000, which was used to produce fine glass powder compacts.

Table 1. Chemical composition in wt% obtained from XRF. The error was $\pm 0.1\%$ based on the standard deviation of four measurements.

Glass	SiO ₂	Na ₂ O	CaO	MgO	Al ₂ O ₃	FeO/Fe ₂ O ₃	K ₂ O	SO ₃	TiO ₂
5000 (fine)	72.2	13.7	9.7	2.4	1.1	0.1	0.5	0.2	0.1
2429 (coarse)	72.2	13.6	9.4	3.3	0.9	0.1	0.3	0.2	0.1

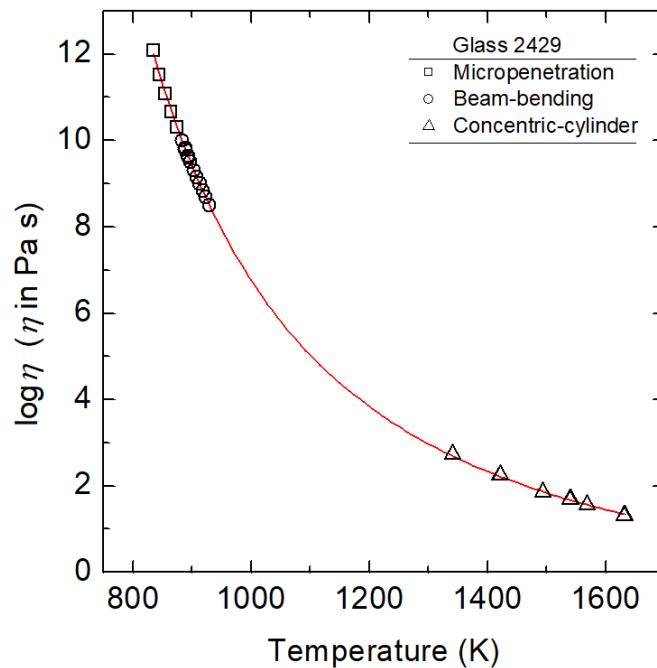


Figure 1. Viscosity of 2429 glass as a function of temperature (symbols) and fit of Eq. (5) to the data (line).

Fig. 2 shows that the surface energy of glass 2429 is constant within the uncertainty of the method for the temperature range studied. The mean value of $342 \pm 5 \text{ mJ m}^{-2}$ agrees quite well with those calculated from the composition [29], [30], [31], [32], [33]. It should be noted that the pendant drop method only provided direct access to surface energy for temperatures above the sintering range. Therefore, this value was also assumed for sintering of glass powder compacts as analysed below.

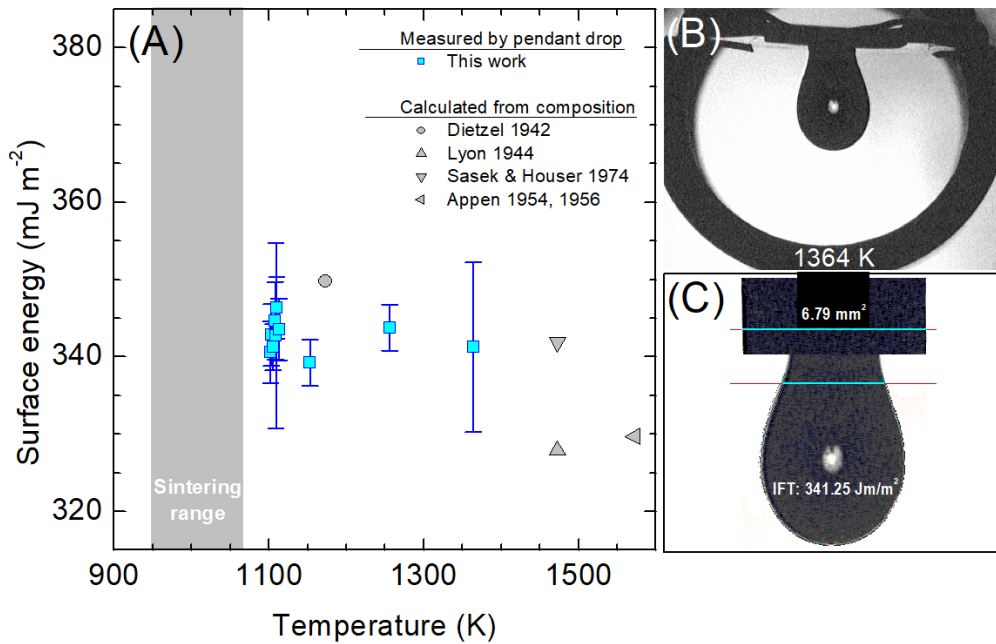


Figure 2. (A) Surface energy in dependence on temperature, (B) contour of the pendant drop at 1364 K recorded in the heating microscope and (C) contour analysis of the part of the drop below the tail marked by the second cyan line and scaled to obtain correct drop volume by first cyan line above the drop (IFT = interfacial tension). Calculation from composition by Dietzel 1942 [29], Lyon 1944 [30], Appen 1954, 1956 [31], [32] and Sasek and Houser 1974 [33].

When comparing the small and large beads before and after different acid-leaching times by electron and optical micrographs, no differences in shape could be detected apart from minor surface damage caused by the manufacturing process. Consequently, acid-leaching resulted in only a slight change in the logarithmically scaled PSD of the fine powder (Fig. 3). For the coarse powder, the changes induced by acid-leaching are likely to be negligible. Attempts to determine them were unsuccessful because the statistical significance of the PSD was too low due to the small number of leached coarse beads. For a better overview, the characteristic quantities of the individual PSD are listed in Tab. 2.

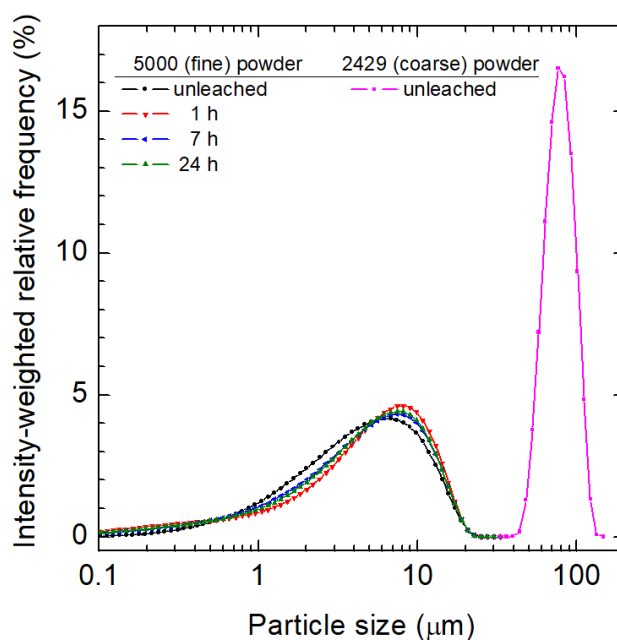


Figure 3. Particle size distribution (PSD) of the fine (5000) and coarse (2429) glass powders under study.

Table 2. Characteristic sizes d_{10} , d_{50} and d_{90} (μm) of the PSD of fine and coarse glass powders for different times of acid-leaching t_{al} (h).

Glass powder	t_{al}	d_{10}	d_{50}	d_{90}
5000 (fine)	0	1.1	4.7	12.2
	1	0.8	5.5	12.9
	7	0.9	5.1	12.7
	24	0.9	5.2	12.7
2429 (coarse)	0	55.8	79.6	102.6

Fig. 4 shows depth profiles of the atomic composition from the surface towards the core of glass beads from fine and coarse glass powders for different leaching times. For clarity, the concentrations have been scaled to their internal values. In each case, a near-surface gradient of the chemical composition was detected. A narrow (10–20 nm) depletion layer of Na, Mg and Ca was already present in the unleached beads. The depth of the altered layer increases with prolonged acid-leaching to about 30–40 nm (Ca and Mg), while Na was depleted up to 150 nm after 24 h of leaching. Note that under acidic conditions rapid cation-proton exchange is to be expected. However, hydrogen-containing species were not measured with SNMS because their ionization probability is low when Kr^+ plasma is used. Therefore, the effect of hydration was determined by thermogravimetry, assuming that all water is released from the hydrated surface layer of the beads in a loose powder bed during heating.

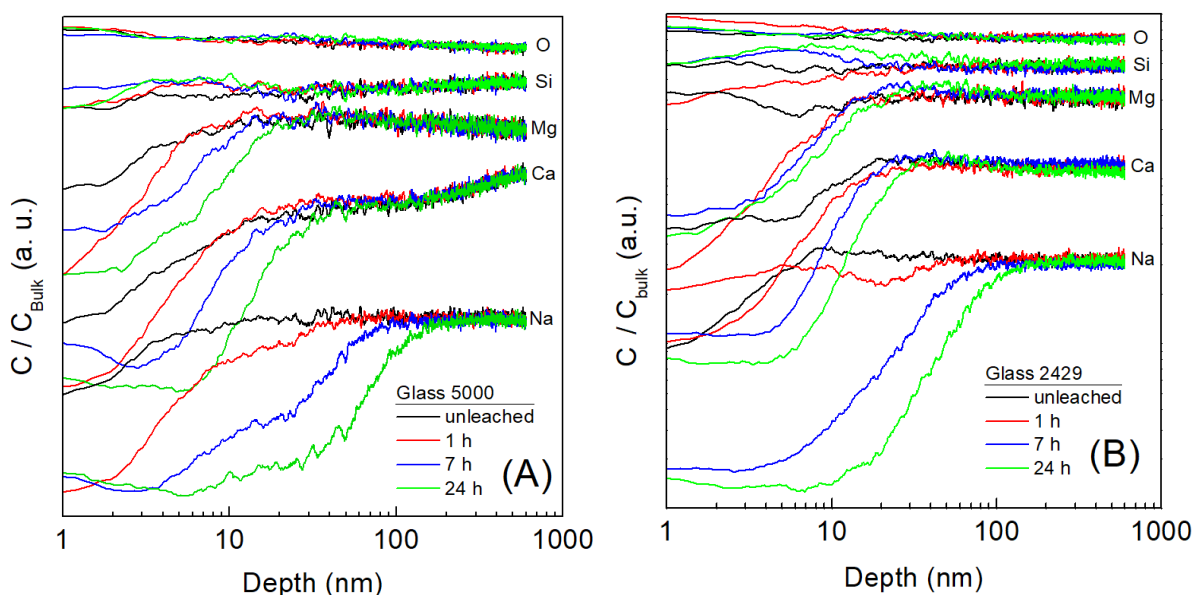
**Figure 4.** Relative atomic composition (scaled by their bulk values) of Na, Ca, Mg, Si and O by SNMS depth profiling. (A) small 5000 and (B) large 2429 glass beads, respectively, for different acid-leaching times. A y-offset is used for clarity.

Fig. 5 shows the weight loss curves of the powders tested. Regardless of the duration of leaching, practically no weight loss is observed for the coarse powders. However, with the fine powders there is a considerable loss of weight, which increases with increasing leaching time. As Fig. 5 exemplifies for the unleached sample, the first weight loss in the range 300–500 K is due to the release of water and some CO_2 , while at higher temperatures (~ 660 K and ~ 790 K) further CO_2 release is detected.

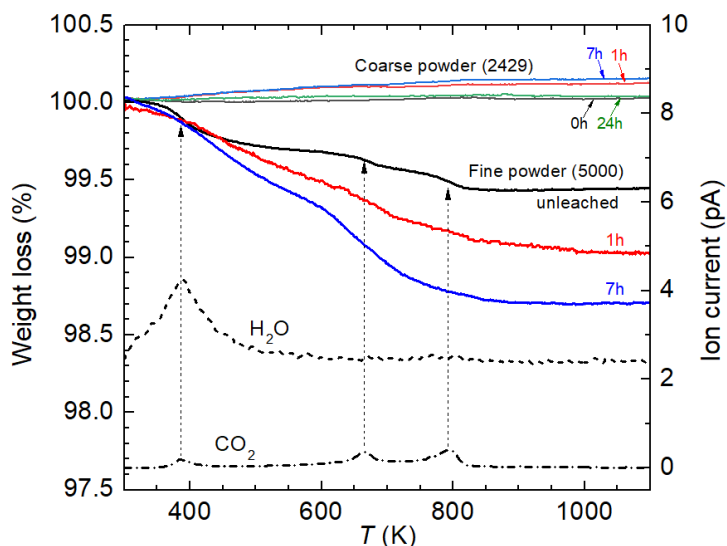


Figure 5. Weight loss (left ordinate) and ion current (right ordinate) of mass 18 (H_2O) and mass 44 (CO_2) for heating fine (5000) and coarse (2429) glass powders for different acid-leaching times at 10 K min^{-1} . The 24 h sample of glass 5000 was not studied.

Fig. 6 shows that heating at 10 K min^{-1} in the DSC does not cause crystallisation at the glass surface until the end of the sintering range (no exothermic events). Small endothermic bumps of the first upscan below the glass transition were attributed to outgassing of volatiles or adsorbed species. The glass transition of the second upscan was used to determine the calorimetric glass transition temperature T_g , as this run was free of thermal history effects. Note the slight difference between the first and second upscan at the beginning of the glass transition, indicating such an artefact of thermal history. For the coarse powder, T_g was found to be constant with leaching time ($840 \pm 3\text{ K}$) and close to the T_{12} determined by viscometry. However, for the fine powder, a small increase of 9 and 12 K was found for leaching times of 7 and 24 hours, respectively. The fact that the glass transition temperature does not depend significantly on the leaching time is due to the negligible (coarse powder) or only slight (fine powder) change in the overall composition of the glass spheres (see approximation of overall composition in the Discussion section).

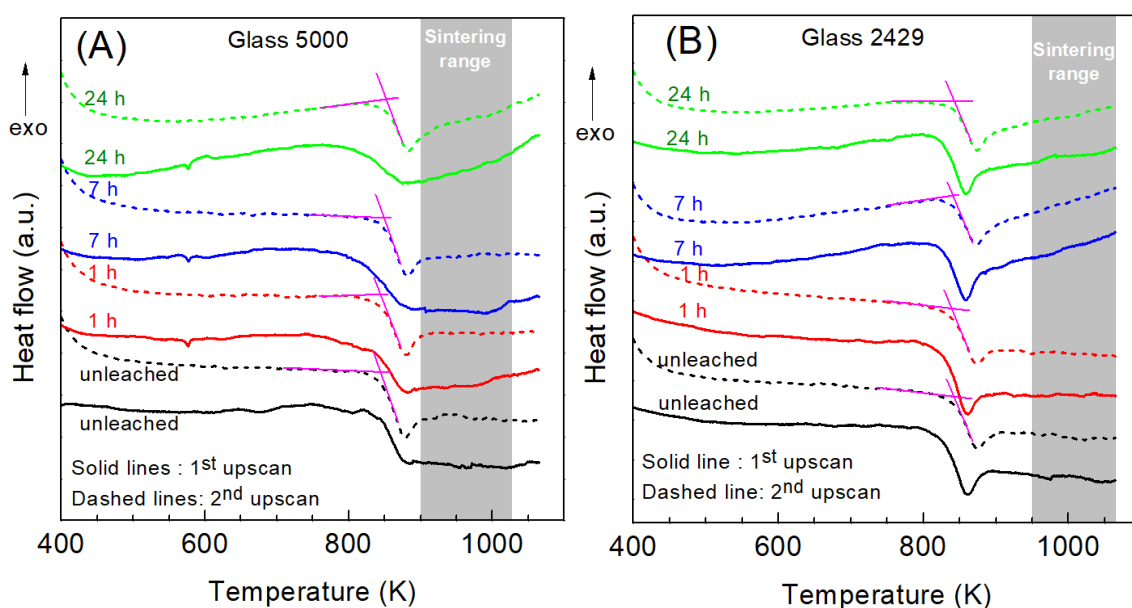


Figure 6. DSC upscans for heating (A) fine 5000 and (B) coarse 2429 glass powders for different acid-leaching times at 10 K min^{-1} . Tangent construction of the 2nd upscan indicates calorimetric T_g . A y-off-set is used for clarity.

Fig. 7 shows images of the powder compact (glass 5000) during heating through the sintering range (923–983 K). The green frame indicates small differences between height and diameter shrinkage, possibly due to influences of the substrate, temperature gradients and gravitational forces. To facilitate comparison of the different treated samples, further analysis was limited to diameter shrinkage. This was also corroborated by the fact that compacts from coarse (2429) glass powders showed some residual porosity (entrapped gases), which led to swelling of the compact at the end of the sintering process, as shown by the volume analysis from the diameter s_d and height s_h shrinkage of the compact (Fig. 8A). Repeated tests show that the influence of the preparation (for compacts made from coarse powders (2429) this was greatest) leads to a scattering of the sintering curve of the compact diameter with respect to the temperature of the inflection point of about 7 K and the final shrinkage of about 1.9 % (Fig. 8B).

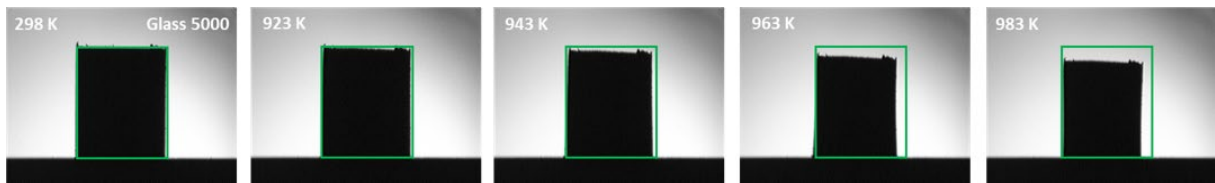


Figure 7. Snapshots of the compact (3 mm diameter) prepared from unleached fine (5000) glass powder in the heating microscope at room temperature (left) and during heating at 10 K min^{-1} through the sintering range. The green frame illustrates the shrinkage of the diameter and height of the compact.

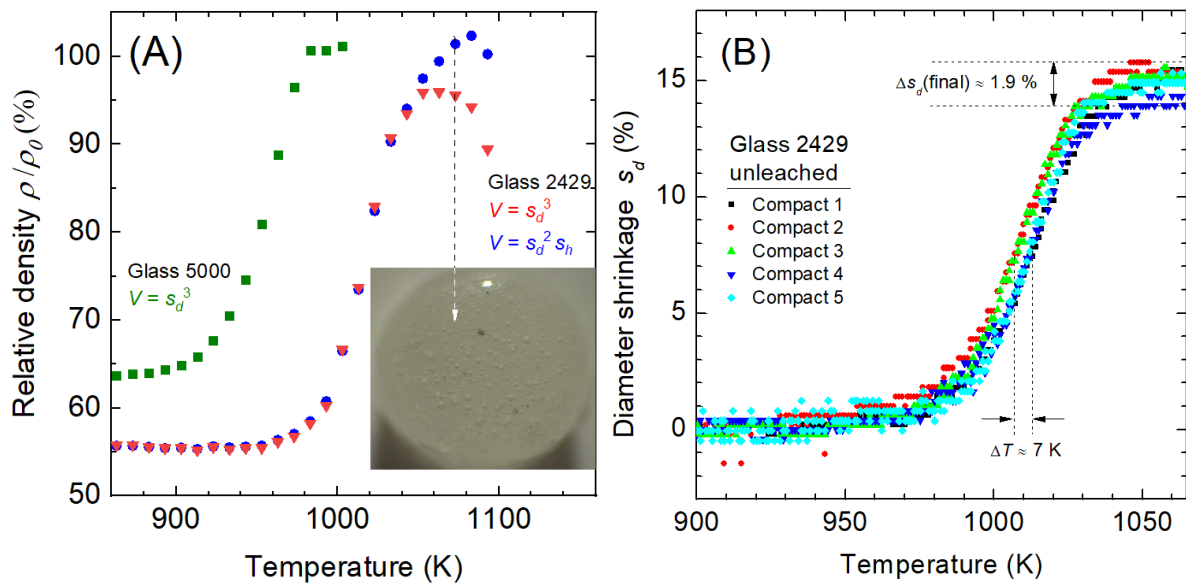


Figure 8. (A) Relative density ρ normalized by the initial “green” density ρ_0 of a compact prepared from fine and coarse glass powders, respectively and (B) diameter shrinkage s_d of 5 compacts prepared from unleached coarse glass powders. The inset of part (A) shows an optical image of the bubble-containing compact (top view) after stopping sintering at 1073 K.

Fig. 9 shows that the diameter shrinkage with increasing leaching time of the glass powders shifts to higher temperatures. For fine glass powder the shift in temperature of the 24 h leached sample relative to the unleached sample is about 45 K, while for coarse powder a shift of about 26 K is determined. In contrast, no trend in the change of the final shrinkage with increasing leaching time is evident.

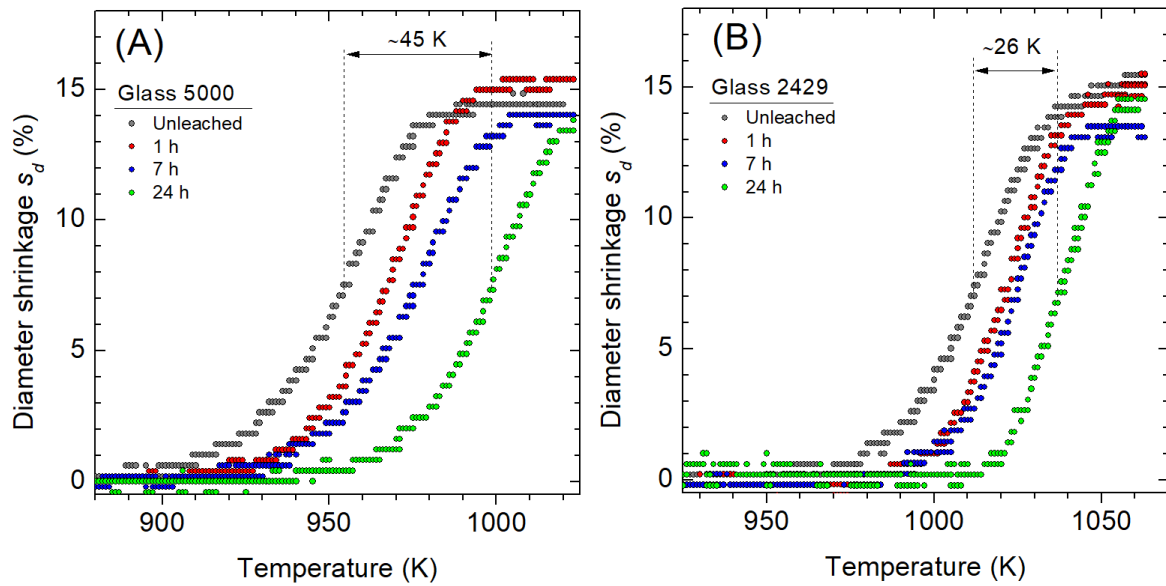


Figure 9. Diameter shrinkage of sintering compacts prepared from (A) fine and (B) coarse glass powders acid-leached for different times.

Fig. 10 shows electron micrographs of samples at the end of the sintering interval made of coarse glass powder that was leached for 24 h on the one hand and not leached on the other. First of all, it becomes clear that the commercial glass beads used show slight variations in the Al-to-Mg ratio, which is the basis for the contrast difference between the sintered beads in both secondary electron images. Due to this chemical heterogeneity, interfaces between the sintered beads could be discerned, but a chemical gradient within the sintered beads as well as near to these interfaces could not be detected. It should be noted that an up to 150 nm thin leaching zone of alkali and alkaline earth ions (see Fig. 4) cannot be resolved with EDXS under the imaging conditions used. In case of Na, a certain triggering of the diffusion seems to be caused by the energy input of the scanning electron beam. Furthermore, due to the still almost spherical shape of the sintered particles, the generated excitation volume could contain a positional shift of the interface and blur it into an interface zone (with respect to the depth of the excitation volume). Therefore, the element maps can only provide integrated information with limited resolution.

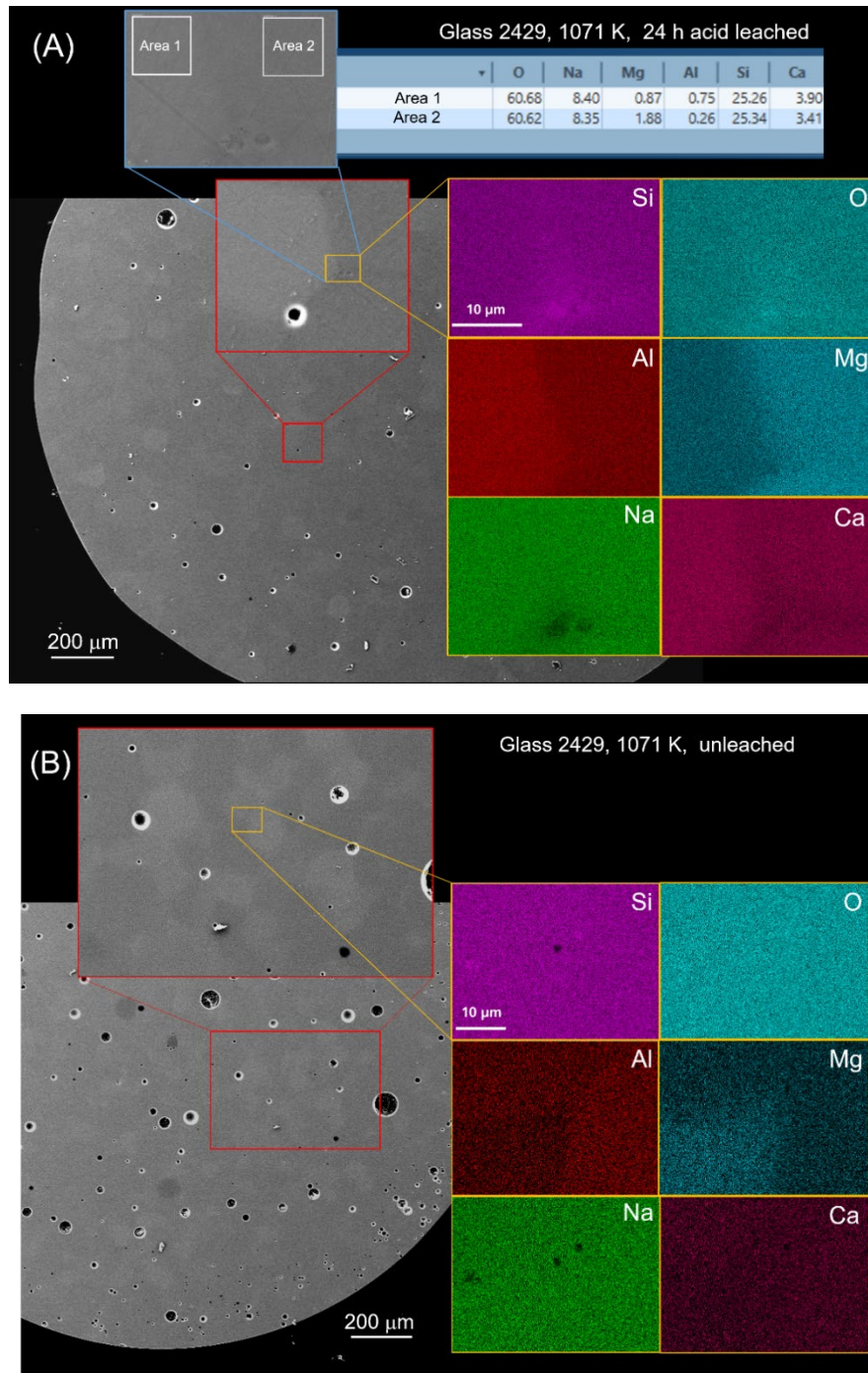


Figure 10. Electron micrographs of the sintered compact (heated to 1071 K) made from (A) 24-hour leached and (B) unleached coarse (2429) glass powder. Radial cross-section at half the height of the compact. Secondary electron imaging (overview) and enlargements (red and blue frames). SEM-EDXS with Si, O, Al, Mg, Na and Ca element maps (orange frames) and chemical composition of areas 1 and 2 (white frames).

4. Discussion

Most strikingly, acid-leaching caused a shift of the sintering range to higher temperatures that was much larger (~ 45 K (glass 5000) and ~ 26 K (glass 2429)) than the scatter caused by the replicate measurements. Surface crystallisation as the cause of this shift could also be ruled out, as exothermic events in the sintering interval were not detected by DSC. To clarify the causes of the shift, the shrinkage was modelled using Eqs. (3) and (4). Therefore, the interfacial energy was assumed to be temperature invariant ($\gamma = 342 \text{ mJ m}^{-2}$), while the temperature-

dependent viscosity was calculated from the MYEGA parameters $A = -1.3$, $m = 38.9$, $T_{12} = 834.3$ K. The PSD of the powders (Fig. 3) was used to specify the relative frequency $\Psi(r_{0j})$ of the sizes r_{0j} . For glass beads, the shape factor $k_f = 1$ was used, while the number of pores per particle O was initially set to ~ 10 ($O^{1/3} = 2.135$) to ensure a continuous slope of the linear shrinkage curve at $t_{0.8}$. Fig. 11 shows that only the steepness of the sintering curve of the unleached coarse powder (dashed line of Fig. 11B) was actually described with this set of parameters. However, T_{12} had to be increased by about 9 K to fit the measured diameter shrinkage, which is only slightly larger than the scatter (7 K) caused by replicate measurements. On the other hand, the sintering curve calculated for the unleached fine powder (dashed line of Fig. 11A) was found to be within the scatter, suggesting that the cluster model approach of Eq. (4), which neglects any interaction between particles of different sizes, is sufficient to describe sintering at all stages.

Despite these limitations of the model for the sintering of unleached powders, the strong delay in the sintering of the leached powders cannot be described with the measured physical parameters of viscosity and interfacial energy of the initial glass. In order to model possible changes in the chemical composition at the surface of the glass spheres, the viscometric glass transition temperature T_{12} and the melting fragility m were treated as adjustable parameters, while the interfacial energy was still considered constant, as its dependence on the chemical composition was estimated to be low. Fig. 11 shows the fitted sintering curves, which lead to higher T_{12} values for all leached glasses with increasing leaching time. At the same time, the somewhat steeper sintering curves cause an increase in m , which is particularly pronounced for the coarse powders.

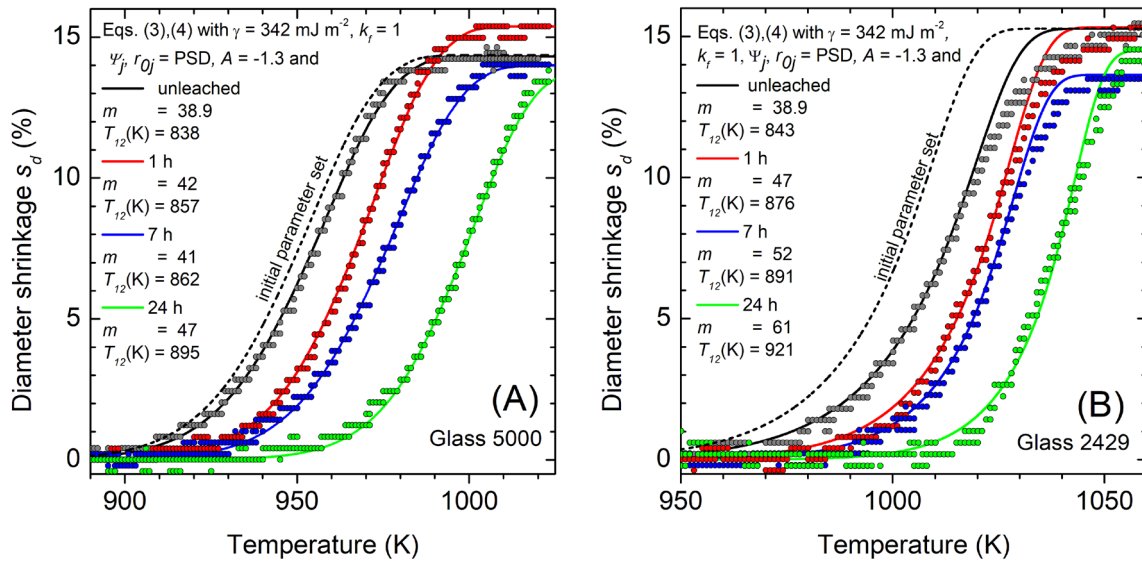


Figure 11. Modelled diameter shrinkage (lines) of sintering compacts prepared from (A) fine and (B) coarse glass powders acid-leached for different times using Eqs. (3) and (4) and the parameters as indicated.

Since the broadness of the sintering curve is closely related to the PSD-dependent cluster model, the predicted increase in m is not considered physically real, also because in silicate glasses a higher glass transition temperature is associated with a decrease in fragility (see, e.g., the difference between the curves of the normalised viscosity of silica glass and soda-lime-silicate glass of the Angell plot [34]). Thus, if the altered chemistry of the surface of the glass spheres, characterised as alkali and alkaline earth depleted (see Fig. 4), is taken as a basis and diffused water is regarded as degassed before sintering (see Fig. 5), a SiO_2 -rich glass melt forms on the surface of the beads with a strongly increased viscosity. One can thus envisage that the glass beads are equipped with a leather-hard surface which, in contact with

each other, only allows mass transport through viscous flow at higher temperatures. This simple picture assumes, of course, that the alkali and alkaline earth concentrations from the core and surface of the sphere do not balance each other out.

The interaction between diffusing atomic species, which balance concentration gradients and sintering was analysed using the ratio of the time scales of diffusive mass transport τ_{Diff} and sintering τ_{Sinter} . The approach was adopted from the analysis of Vasseur et al. [18] for diffusive mass transport during sintering of hydrous glasses. It is based, on the one hand, on the time required for mass transport to equilibrate the concentration gradients $t_{Diff} = 1/\tau_{Diff} = \lambda_{Diff}^2/D$ with the effective diffusion length λ_{Diff} and $D =$ diffusion coefficient, and, on the other hand, on the time for concurrent sintering, which according to Eq. (1) is $t_{Sinter} = 1/\tau_{Sinter} = r_0\eta/\gamma$. Thus, for isochronous heating and for $\lambda_{Diff} = r_0$, one can therefore integrate [18]:

$$\frac{\tau_{Diff}}{\tau_{Sinter}} = \frac{\frac{1}{r_0^2} \int_0^t D dt}{\frac{\gamma}{r_0} \int_0^{t_1} dt} \quad (6)$$

For $\tau_{Diff} \gg \tau_{Sinter}$, diffusive mass transport can balance different concentrations of chemical components at the surface and in the core of the acid leached glass spheres before sintering, since up to $t_{0.8}$ there is an open porosity and the effective diffusion length λ_{Diff} can be approximated with the initial radius r_0 of the glass beads. For longer times, there is a closed porosity in the sintered compact and the effective diffusion length jumps to the size of the sintered body. In contrast, sintering at $\tau_{Diff} \ll \tau_{Sinter}$ prevents the balancing of chemical gradients within the glass beads and altered surface layers can control the sintering kinetics.

We have analysed in Fig. 12 three different types of mobile atomic species (Ca^{2+} , Na^+ and H_2O) of the soda-lime-silicate glass structure in terms of their much shorter relaxation times than those of viscous flow [35], [36]. The temperature-dependent effective water diffusion coefficient was taken from the review by Shelby [37], while the tracer-diffusivities of ^{22}Na and ^{45}Ca were used from the study of Mehrer et al. [35]. The effective diffusion length λ was analysed for the radii of the three characteristic particle sizes d_{10} , d_{50} and d_{90} of the PSD of fine and coarse powders (see Tab. 2). In case of water diffusivity, dehydration of the acid leached surface layer (thickness up to 150 nm) was also considered as the partial vapour pressure during heating of the powder compacts differs from the water content in the glass. Fig. 12A shows that for fine powders, diffusion of water species and sodium ions is effective before the start of sintering, while calcium depletion at the surface of the glass beads after acid leaching can persist in the sinter interval as diffusion from the core cannot reach the surface. In contrast, water diffusivity can also affect the sintering of the coarse powders (Fig. 12B). At $\tau_{Diff} \ll \tau_{Sinter}$, water cannot diffuse effectively from the sintered compact and can contribute to the observed gas bubble formation (see inset of Fig. 8A). Fig. 12B, however, shows also that dehydration of the surface layer is still effective because the diffusion length of 150 nm is significantly smaller than r_0 . The water diffusivity analysis is in principle consistent with the observed mass loss and degassing (of H_2O) of the fine powder during heating (see Fig. 5), while no mass loss or degassing activity was measured for the coarse powder. Of course, it should be noted that the absence of a mass loss signal may also be due to the much lower total amount of water dissolved in the acid leached layers of the coarse powder (detection limit).

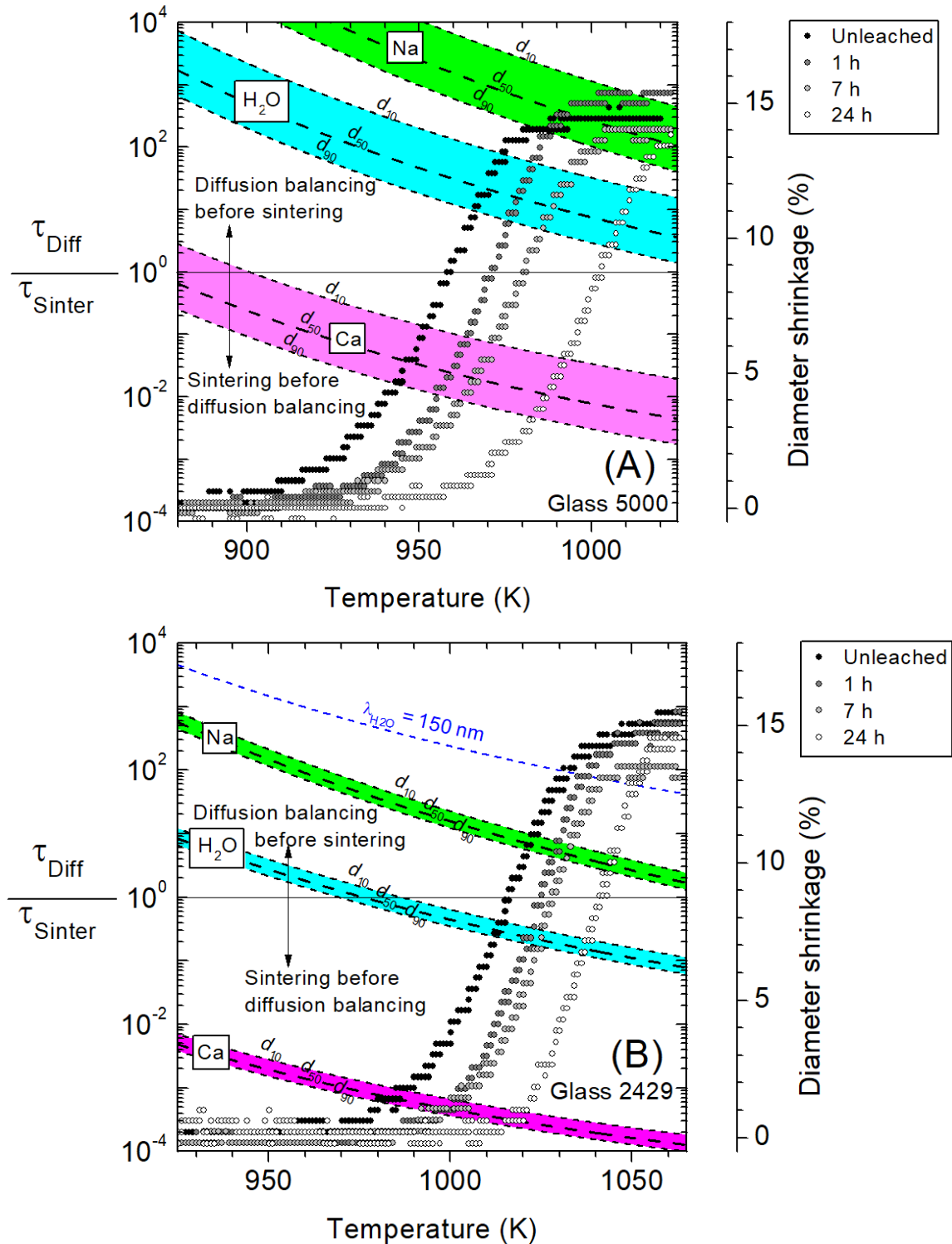


Figure 12. τ_{Diff} -to- τ_{Sinter} ratio (dashed lines) of Na^+ , H_2O and Ca^{2+} for different diffusion lengths (d_{10} , d_{50} and d_{90}) and diameter shrinkage of sintering compacts prepared from (A) fine 5000 and (B) coarse 2429 glass powders acid-leached for different times.

While diffusing Na^+ ions can compensate for concentration differences before sintering, the total amount decreases with increasing leaching time, as Na^+ is enriched in the leachant. A rough calculation of the mass balance shows that this effect can contribute up to 2.4 mol% Na_2O for the fine powder (assuming a glass bead of $4.7 \mu m$ diameter (d_{50}) consisting of a 150 nm thick Na^+ -free layer on the surface, while the initial concentration of 13.2 mol% Na_2O is present underneath and layer and core glass are of same density).

5. Conclusions

Acid-leaching of soda-lime-silicate glass powders leads to ion exchange processes at the particle surfaces. The interdiffusion of alkali and alkaline earth ions with protons of the acid leads to a hydrated surface layer depleted in Na^+ , Ca^{2+} and Mg^{2+} . With increasing leaching time, the thickness of the altered surface layer increases and the shrinkage curve shifts to higher temperatures. The latter (shrinkage curve shift), is more pronounced for the fine glass powders. In order to explain the sintering delay of the acid leached powders, a modelling of the shrinkage curves with adjustable viscosity parameters (viscometric glass transition T_{12} and kinetic fragility m) was carried out, which shows that T_{12} increases with the leaching time. The simulated increase of m was not considered physically real, as the width of the sintering curve was closely related to the PSD-dependent cluster model used, among other factors. Possible interactions between diffusing atomic species (Na^+ , H_2O and Ca^{2+}), which can compensate for concentration differences within the glass powder beads, and sintering were analysed for constant heating using the ratio of the time scales of diffusive mass transport and sintering. It was found that for both powder series (fine and coarse), the depletion of alkaline earth ions (Ca^{2+}) in the altered surface layer persists during the sinter interval, while the sodium ion concentration in the glass beads is already balanced before sintering starts. The effect of water diffusivity is negligible in the case of the fine powder (degassing and mass loss before sintering), while it cannot be completely ruled out for the coarse powder. The sintering retardation can therefore be described as the effect of a composition gradient, which in turn leads to a viscosity gradient, whereby the outer part of the glass beads is less prone to viscous flow due to the higher silica content and the lower amount of modifiers. As the total amount of Na^+ ions exchanged increases with increasing leaching time, the Na^+ concentration remaining in the glass spheres decreases, further increasing the effective viscosity at the surface.

Data availability statement

Data will be made available on request.

Author contributions

R. Gomes-Fernandes: Conceptualization, Methodology, Formal analysis, Investigation, Visualization, Writing – original draft, Writing – review & editing. R. Al-Mukadam: Methodology, Formal analysis, Investigation, Writing – review & editing. H. Bornhöft: Methodology, Formal analysis, Investigation, S. Reinsch: Methodology, Formal analysis, Investigation. R. Müller: Formal Analysis, Validation, Visualization, Writing – review & editing. S. Selle: Funding acquisition, Project administration, Resources, Supervision, Writing – review & editing. J. Deubener: Funding acquisition, Project administration, Resources, Supervision, Validation, Visualization, Writing – review & editing.

Competing interests

The authors declare that they have no competing interests.

Funding

J.D. and S.S. thanks the Deutsche Forschungsgemeinschaft (DFG) for providing funding under grant DE 598/30-1 and SE 2796/2-1, respectively.

References

- [1] A. Shenoy, N. Shenoy, "Dental ceramics: An update", *J. Conserv. Dent.*, vol. 13, pp. 195–203, 2010, doi: <https://doi.org/10.4103/0972-0707.73379>.
- [2] E. D. Zanotto, "A bright future for glass-ceramics", *J. Am. Ceram. Soc. Bull.*, vol. 89, pp. 19–27, 2010.
- [3] P. Colombo, G. Brusatin, E. Bernardo, G. Scarinci, "Inertization and reuse of waste materials by vitrification and fabrication of glass-based products", *Cur. Op. Solid State Mater. Sci.*, vol. 7, pp. 225–239, 2003, doi: <https://doi.org/10.1016/j.cossms.2003.08.002>.
- [4] R. G. Frieser, "A review of solder glasses", *Electrocomp. Sci. Technol.*, vol. 2, pp. 163–199, 1975, doi: <https://doi.org/10.1155/APEC.2.163>.
- [5] R. Müller, S. Reinsch, "Viscous-phase silicate processing", in: N. P. Bansal, A. R. Boccacini (eds.) *Ceramic and composites processing methods*, Wiley, Hoboken, 2012, pp. 75–144, doi: <https://doi.org/10.1002/9781118176665.ch3>.
- [6] J. Kim, S. Hwang, W. Sung, H. Kim, "Thermal and dielectric properties of glass-ceramics sintered based on diopside and anorthite composition", *J. Electroceram.*, vol. 23 pp. 209–213, 2009, doi: <https://doi.org/10.1007/s10832-007-9395-9>.
- [7] M. T. Sebastian, H. Jantunen, "Low loss dielectric materials for LTCC applications: a review", *Int. Mat. Rev.*, vol. 53, pp. 57–90, 2008, doi: <https://doi.org/10.1179/174328008X277524>.
- [8] H. Elsayed, M. Picicco, A. Dasan, J. Kraxner, D. Galusek, E. Bernardo, "Glass powders and reactive silicone binder: application to digital light processing of bioactive glass-ceramic scaffolds", *Ceram. Inter.*, vol. 46, pp. 25299–25305, 2020, doi: <https://doi.org/10.1016/j.ceramint.2020.06.323>.
- [9] A. Dasan, P. Ožóg, J. Kraxner, H. Elsayed, E. Colusso, L. Grigolato, G. Savio, D. Galusek, E. Bernardo, "Up-Cycling of LCD Glass by Additive Manufacturing of Porous Translucent Glass Scaffolds", *Materials*, vol. 14, Art. no. 5083, 2022, doi: <https://doi.org/10.3390/ma14175083>.
- [10] S. Pagliuca, W. D. Faust, "Porcelain (Vitreous) enamels and industrial enameling processes - The preparation, application, and properties of enamels", IEI, Montova, 2011, pp. 432–492.
- [11] S. Rossi, C. Zanella, R. Sommerhuber, "Influence of mill additives on vitreous enamel properties", *Mater. Des.*, vol. 55, pp. 880–887, 2014, doi: <https://doi.org/10.1016/j.matdes.2013.10.059>.
- [12] R. Conradt, "Chemical durability of oxide glasses in aqueous solution: a review", *J. Am. Ceram. Soc.*, vol. 91, pp. 728–735, 2008, doi: <https://doi.org/10.1111/j.1551-2916.2007.02101.x>.
- [13] C. M. Jantzen, K. G. Brown, J. B. Pickett, "Durable glass for thousands of years", *Int. J. Appl. Glass Sci.*, vol. 1, pp. 38–62, 2010, doi: <https://doi.org/10.1111/j.2041-1294.2010.00007.x>.
- [14] R. W. Douglas, T. M. M. El-Shamy, "Reactions of glasses with aqueous solutions", *J. Am. Ceram. Soc.*, vol. 50, pp. 1–8, 1967, doi: <https://doi.org/10.1111/j.1151-2916.1967.tb14960.x>.
- [15] R. Doremus, "Interdiffusion of hydrogen and alkali ions in a glass surface", *J. Non-Cryst. Solids*, vol. 19, pp. 137–144, 1975, doi: [https://doi.org/10.1016/0022-3093\(75\)90079-4](https://doi.org/10.1016/0022-3093(75)90079-4).
- [16] H. Scholze, "Chemical durability of glasses", *J. Non-Cryst. Solids*, vol. 52, pp. 91–103, 1982, doi: [https://doi.org/10.1016/0022-3093\(82\)90283-6](https://doi.org/10.1016/0022-3093(82)90283-6).
- [17] E. Bernardo, G. Scarinci, S. Hreglich, G. Zangiaccomi, "Effect of time and furnace atmosphere on the sintering of glasses from dismantled cathode ray tubes", *J. Eur. Ceram. Soc.*, vol. 27, pp. 1637–1643, 2006, doi: <https://doi.org/10.1016/j.jeurceramsoc.2006.04.144>.
- [18] J. Vasseur, F.B. Wadsworth, Y. Lavallée, D.B. Dingwell, "Dehydration-driven mass loss from packs of sintering hydrous silicate glass particles", *J. Am. Ceram. Soc.*, vol. 106, pp. 4643–4653, 2023, doi: <https://doi.org/10.1111/jace.19120>.
- [19] K. Shandarova, G. Hensch, J. Deubener, W. Dziony, L. Wondraczek, "Improving the corrosion resistance of sol-gel-derived aluminoborosilicate glass coatings by nitridation", *J.*

- Non-Cryst. Solids, vol. 447, pp. 171–177, 2016, doi: <https://doi.org/10.1016/j.jnoncrysol.2016.06.016>.
- [20] J. Frenkel, “Viscous flow of crystalline bodies under the action of surface tension”, *J. Phys. (USSR)*, vol. 9, pp. 385–391, 1945.
- [21] V. V. Skorokhod, “Development of the ideas of Ya. I. Frenkel' in the contemporary rheological theory of sintering”, *Powder Metall. Met. Ceram.*, vol. 34, pp. 521–527, 1996, doi: <https://doi.org/10.1007/BF00559961>.
- [22] J. K. Mackenzie, R. Shuttleworth, “A phenomenological theory of sintering”, *Proc. Phys. Soc. B.*, vol. 62, pp. 833–852, 1949, doi: <https://doi.org/10.1088/0370-1301/62/12/310>.
- [23] R. Müller, “On the kinetics of sintering and crystallization of glass powders”, *Glastech. Ber. Glass. Sci. Technol.* vol. 67 C, pp. 93–98, 1994.
- [24] M. O. Prado, E.D. Zanotto, R. Müller, “Model for sintering polydispersed glass particles”, *J. Non-Cryst. Solids*, vol. 279, pp.169–178, 2001, doi: [https://doi.org/10.1016/S0022-3093\(00\)00399-9](https://doi.org/10.1016/S0022-3093(00)00399-9).
- [25] J. Deubener, H. Bornhoft, S. Reinsch, R. Müller, J. Lumeau, L.N. Glebova, L.B. Glebov, “Viscosity, relaxation and elastic properties of photo-thermo-refractive glass”, *J. Non-Cryst. Solids*, vol. 355, pp. 126–131, 2009, doi: <https://doi.org/10.1016/j.jnoncrysol.2008.10.002>.
- [26] D. Di Genova, A. Zandona, J. Deubener, “Unravelling the effect of nano-heterogeneity on the viscosity of silicate melts: Implications for glass manufacturing and volcanic eruptions”, *J. Non. Cryst. Solids* vol. 545, Art. no. 120248, 2020, doi: <https://doi.org/10.1016/j.jnoncrysol.2020.120248>.
- [27] G. Meerlender, “Viskositäts-Temperaturverhalten des Standardglases I der DGG“, *Glastech. Ber.*, vol. 47, pp. 1–3, 1974.
- [28] J. C. Mauro, Y. Yue, A. J. Ellison, P. K. Gupta, D. C. Allan, “Viscosity of glass-forming liquids”, *Proc. Natl. Acad. Sci. U.S.A.*, vol. 106, pp. 19780–19784, 2009, doi: <https://doi.org/10.1073/pnas.0911705106>.
- [29] A. Dietzel, “Praktische Bedeutung von Berechnung der Oberflächenspannung von Gläsern, Glasuren und Emails“, *Sprechsaal*, vol. 75, pp. 82–85, 1942.
- [30] K. C. Lyon, “Calculation of surface tensions of glasses”, *J. Am. Ceram. Soc.*, vol. 27, pp. 186–189, 1944, doi: <https://doi.org/10.1111/j.1151-2916.1944.tb14889.x>.
- [31] A. A. Appen, “Versuch zur Klassifizierung von Komponenten nach ihrem Einfluß auf die Oberflächenspannung von Silikatschmelzen“, *Silikattechn.*, vol. 5, pp. 11–12, 1954.
- [32] A. A. Appen, “Some "anomalies" in the properties of glass”, *Travaux du IVe congres international du verre, Paris*, 1956, pp. 36–40.
- [33] L. Šašek, M. Houser, “Application of mathematico-statistical methods in silicate research. 3. Determination of mathematical relations for computing the temperature dependence of surface tension and chemical composition in the field of sheet and container glass”, *Sb. Vys. Sk. Chem.-Technol. Praze Chem. Technol. Silik.*, vol. L5, pp. 49–84, 1974.
- [34] C. A. Angell, “Spectroscopy simulation and scattering, and the medium range order problem in glass”, *J. Non-Cryst. Solids*, vol. 73, pp. 1–17, 1985, doi: [https://doi.org/10.1016/0022-3093\(85\)90334-5](https://doi.org/10.1016/0022-3093(85)90334-5).
- [35] H. Mehrer, A. W. Imre, E. Tanguiep-Nijokep, “Diffusion and ionic conduction in oxide glasses”, *J. Phys.: Conf. Series*, vol. 106, Art. no. 012001, 2008, doi: <https://doi.org/10.1088/1742-6596/106/1/012001>.
- [36] S. Reinsch, R. Müller, J. Deubener, H. Behrens, “Internal friction of hydrated soda-lime-silicate glasses”, *J. Chem Phys.*, vol. 139, Art. no. 174506, 2013. doi: <https://doi.org/10.1063/1.4828740>.
- [37] J. E. Shelby, “A limited review of water diffusivity and solubility in glasses and melts”, *J. Am. Ceram. Soc.*, vol. 91, pp. 703–708, 2008, doi: <https://doi.org/10.1111/j.1551-2916.2007.01946.x>.